Event-chain Monte Carlo simulations of liquid crystalline phase transitions of hard triangles

Antonia J. Bock[1], Felix S. Kratz[1], Tobias A. Kampmann[1] and Jan Kierfeld[1] [(a)]

[1] *Department of Physics, TU Dortmund University - Dortmund, Germany*

Abstract – We extend the rejection-free event-chain Monte Carlo approach to a liquid crystal system consisting of infinitely thin hard triangles. This triangle liquid crystal behaves very similar to hard circular platelets, which are an important model system for discotic liquid crystals. We investigate the isotropic-nematic phase transition of the triangle liquid crystal in detail measuring orientational order parameter, susceptibility, and equation of state. Our results suggest that the transition is discontinuous. In the event-chain Monte Carlo simulation, we treat the three vertices of triangles as relevant degrees of freedom and derive lifting probabilities that guarantee maximal global balance of the algorithm. We also present a novel approach to derive the lifting probabilities from diffusional splitting probabilities on the hard object. We achieve significant performance gains over standard local Monte Carlo techniques, which we substantiate by comparing autocorrelation times. With the application to triangular liquid crystals, we present the first event-chain Monte Carlo simulation of surface-like objects, which extends the scope of the event-chain Monte Carlo technique considerably. The lifting rules derived for isolated triangles will also be applicable to extended triangulated surfaces.

Introduction. – Monte Carlo (MC) and molecular dynamics are the main simulation techniques for many-particle systems [1,2]. For steric particle interactions, MC simulations are easier to implement. The standard Markov chain MC (MCMC) algorithm is the Metropolis-Hastings algorithm, which is based on the concept of detailed balance [3, 4]. For steric systems, it simply proposes to locally displace a particle and to reject in case of overlaps. In dense systems, local MC simulations become ineffective as the acceptance ratio of the proposed displacements becomes very small. Cluster MCMC algorithms (such as the Wolff or Swendsen-Wang algorithms for lattice spin systems [5, 6]) attempt to update whole clusters of particles within a single MCMC move while still maintaining detailed balance. Starting from hard-sphere systems, the event-chain MC (ECMC) algorithm has been established as a cluster MC algorithm; it is rejection-free and based on global rather than detailed balance [7,8]. In such systems, the ECMC algorithm constructs a chain of hard spheres, which is moved as a cluster by a simple "billiard"-like procedure. The absence of rejections is achieved by so-called *lifting* moves, which transfer the event-chain (EC) to other particles or change its direction instead of triggering rejections.

[(a)] E-mail: jan.kierfeld@tu-dortmund.de

In the past years, ECMC simulations and variants, such as the Newtonian ECMC [9], have advanced to a versatile simulation technique by generalizing to arbitrary "soft" particle [10] and many-particle interactions [11]. They have proven high efficiency in equilibrating many types of dense soft-matter [12] and molecular systems [13].

So far, ECMC simulations of geometrically more challenging objects, such as surfaces or membranes embedded in three-dimensional space, have not been attempted. In the presented work, we will take a first step towards this and apply the ECMC technique to a dense system of infinitely thin but impenetrable hard triangles, which are obviously the simplest type of surface-like objects. We parametrize the triangular platelets by the position of their three vertices and allow the triangle edges to change their length by $\pm 30\%$ in order to facilitate vertex moves. We formulate an EC lifting scheme that handles triangle collisions constituting effective 4-particle interactions and that allows global balance to be achieved and proven. This enables us to efficiently equilibrate highly dense triangle systems, such as the system shown in fig. 1.

From a physics perspective, ECMC provides an ideal tool to study liquid-crystalline ordering of such triangular platelets [14]. We study their nematic ordering and demonstrate that the ECMC algorithm allows for an ef-

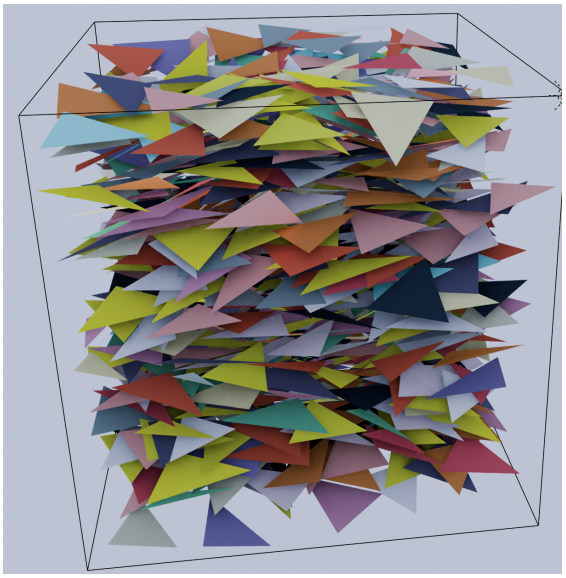

Fig. 1: ECMC simulation snapshot of infinitely thin hard triangles in the nematic phase at $\eta = 3.19 \pm 0.03$, with $N = 1793$ triangles and box length $L = 5a$.

fective equilibration through this phase transition. In the context of discotic liquid crystals, the phase behavior of platelets is of long-standing interest in colloidal science with various applications [15, 16]. We show that ECMC simulations provide a new and effective simulation method for these systems.

Model. – We consider N triangles in a box of volume $V = L^3$ which obeys periodic boundary conditions. Each triangle is infinitely thin and spanned by three point-like "particles" (vertices). Initially, they all have the same distance a implying equilateral triangles of an area $A = \sqrt{3}/4a^2$. The surface of a triangle is impenetrable for other triangles, i.e., there are steric interactions both between a vertex of one triangle and the surface of a second triangle and between two edges of two different triangles. This gives rise to effective 4-particle interactions between vertices.

Comparable publications on systems containing hard triangles like these are lacking. Nonetheless, there exist studies done on hard disk-like platelets simulated with local MC methods [14, 17]. A naive approach to compare the results on differently shaped platelets in 3D-space is achieved by employing a unitless packing fraction $\eta = A^{3/2}N/V$ which does not include the specific shape but the area (therefore, $\eta > 1$ is possible). As the triangles' area changes during the simulation due to their flexible edge lengths (A actually reduces for entropic reasons), we characterize the system by its average area $\langle A\rangle$ and its corresponding packing fraction $\eta \equiv \langle A\rangle^{3/2}N/V$ (we could also use $\eta' = \langle A^{3/2}\rangle N/V$, which is ca. 3% bigger in the density range considered).

ECMC algorithm. – The ECMC algorithm for hard triangles works as follows: each vertex is treated as a particle with radius zero, and three vertices span the steric surface of the triangle. To make single vertex moves possible, the edges are allowed to vary their length by $\pm 30\%$ (this excludes the possibility that edges shrink to zero length).

The key concept of ECMC simulations is to enlarge the state space of physical configurations by an additional lifting variable (in particle-based simulations, this is the index of the "active" or moving particle). In an EC, standard local MC rejections are "redirected" into changes of the lifting variable (i.e., the EC continues with the next active particle that has been lifted to) with probabilities such that global probability flux balance remains intact [12].

For pair interactions, such as a hard-sphere interaction, there is only one interaction partner to lift to. For $\mathcal{N}$-particle interactions, however, there are up to $\mathcal{N}-1$ interaction partners and, thus, possibilities to perform the lifting. We need to determine lifting probabilities λ_{ij} to lift from the active particle i to one of the rejection-causing particles j in such a way that global balance is guaranteed [11]. The correct lifting probabilities are crucial and will be derived in the following section.

Then, the ECMC algorithm for *hard triangles* comprises the following steps:

1. Initialize a valid configuration, i.e., with no overlap, of N triangles in a volume V, and choose an EC displacement length w;
2. start an EC: choose a random particle i, the so-called active vertex; choose a random EC direction $\vec{e}_w$;
3. find the shortest rejection distance r: find out how far i can be moved until a rejection is caused by a set M of vertices containing i, either by collision or by an edge becoming too long/short;
   (a) if $r < w$: move i by $r\vec{e}_w$, reduce the displacement length, $w \to w - r$, and perform the lifting move: choose the next active particle j by sampling the probability distribution from $\lambda_{i\{j\}}$ with $j \in M \setminus \{i\}$; go to step 3;
   (b) if $r \geq w$: move i by $w\vec{e}_w$; go to step 2.

Theoretical background. The ECMC algorithm is a cluster algorithm based on global balance. It is rejection-free, and probability currents between states are unidirectional. These two properties define *maximal global balance*.

All MCMC algorithms aim to sample states α with the Boltzmann probability $\pi(\alpha) = \exp\{-E(\alpha)\}$ (in natural units $\mathrm{k_B}T = 1$) via a Markov chain, which is characterized by transition rates $p(\alpha \to \beta)$ between two states α and β. Probabilities $\pi(\alpha)$ and transition rates $p(\alpha \to \beta)$ induce probability currents $\phi(\alpha \to \beta) \sim \pi(\alpha)p(\alpha \to \beta)$. For the correct sampling of the Boltzmann distribution, the *global balance condition* $\pi(\alpha) = \sum_\beta \phi(\beta \to \alpha) = \sum_\gamma \phi(\alpha \to \gamma)$ is sufficient. Standard Metropolis MC, as defined by the transition rates $p^{\mathrm{Metr}}(\alpha \to \beta) = \exp\{-[\sum_M \Delta E_M(\alpha \to \beta)]^+\}$ (with $[x]^+ \equiv \max\{0, x\}$) [3, 4], also fulfills the stronger condition of detailed balance, $\phi(\alpha \to \beta) = \phi(\beta \to$

α) for all α, β.

The ECMC algorithm uses the *factorized Metropolis filter* [10] $p^{\text{fact}}(\alpha \to \beta) = \exp\{-\sum_M [\Delta E_M(\alpha \to \beta)]^+\}$ for physical transitions between different configurations; this becomes identical to the standard Metropolis filter for steric interactions and also obeys detailed balance. In the limit of infinitesimal moves (and correspondingly infinitesimal energy changes), the rejection probability is given by

$$1 - p^{\text{fact}}(\alpha \to \beta) = \sum_M [dE_M(\alpha \to \beta)]^+ , \qquad (1)$$

and a rejection is always caused by only a single interaction at a time, the rejection-causing factor M.

The state space is extended by the lifting variable i denoting the active particle, which is the only particle that can move. The lifting variable will be used to "redirect" all rejection flows into *lifting flows*, which change the active particle and make ECMC *rejection-free* by construction. We consider a fixed infinitesimal move $d\vec{w} = dw\vec{e}_w$ of the active particle i giving rise to a change of the physical configuration $\alpha_i \to \beta_i$. We define $+dE_{i,M}$ as the corresponding energy change in a factor M with $i \in M$. According to (1), each factor M with $i \in M$ causes a rejection with probability $[dE_{i,M}]^+$. For hard particles, this entails that the next collision causes rejection.

For pairwise interactions ($\mathcal{N} = 2$), there is a unique collision or rejection-causing partner $k \in M \setminus \{i\}$, to which the EC is lifted with a probability $p_M^{\text{lift}}(\alpha_i \to \alpha_k) = [dE_{i,M}]^+$ identical to the rejection probability. In case of $\mathcal{N}$-particle interactions, we lift to any of the $\mathcal{N}-1$ collision partners k with total probability

$$p_M^{\text{lift}}(\alpha_i \to \alpha_M) = \sum_{k \in M \setminus \{i\}} p_M^{\text{lift}}(\alpha_i \to \alpha_k) = [dE_{i,M}]^+ . \quad (2)$$

Then, we still have to determine to which of the remaining $\mathcal{N}-1$ particles $k(\neq i)$ we lift, and we decompose $p_M^{\text{lift}}(\alpha_i \to \alpha_k) = [dE_{i,M}]^+ \lambda_{ik}$ with the conditional probability λ_{ik} to lift to $k \in M \setminus \{i\}$ if $M \ni i$ caused a rejection [11].

Lifting will always occur from a particle i with $dE_{i,M} > 0$ (triggering the lifting) to a particle k with $dE_{k,M} < 0$. In ref. [11], it has been derived that global balance is fulfilled if

$$\sum_{i \in M \setminus \{k\}} [dE_{k,M}]^+ \lambda_{ik} = [-dE_{k,M}]^+ , \qquad (3)$$

which has to be solved together with the normalization condition $\sum_{k \in M \setminus \{i\}} \lambda_{ik} = 1$. This results in

$$\lambda_{ik} = \frac{[-dE_{k,M}]^+}{\sum_{l \in M} [-dE_{l,M}]^+} = \frac{[-dE_{k,M}]^+}{\sum_{l \in M} [dE_{l,M}]^+}, \qquad (4)$$

where the last equality holds because of energy conservation $\sum_{l \in M} dE_{l,M} = 0$. This determines the lifting probabilities λ_{ik} uniquely for $\mathcal{N} \leq 3$. For $\mathcal{N} \geq 4$, the result (4) is not unique but the most symmetric choice fulfilling also $\lambda_{ik} = \lambda_{jk}$ for all $i, j \in M$. Interpreting energy changes dE as *opposing* forces in EC direction, the finding in (4) can be rephrased such that an opposing force on particle i triggers lifting of the EC to a particle k with *supporting* force in EC-direction and with a conditional probability λ_{ik} proportional to the supporting force.

Deriving the lifting probabilities for triangles. – For hard triangles, an active vertex i triggers a rejection if:

1. an edge ij connecting vertex i with another vertex j exceeds or falls bewlow the allowed length;
2. vertex i hits the surface of a triangle spanned by jkl ("vertex hits surface");
3. an edge im hits an edge jk of another triangle ("edge hits edge").

The case of an edge hitting a surface needs no separate consideration because it is contained in case 3. Case 1 results from a pairwise interaction ij such that it is clear that we lift $i \to j$. The rejections in cases 2 and 3, however, involve $\mathcal{N} = 4$ particles (the rejection-causing factor is $M = \{i, j, k, l\}$). We derive the corresponding lifting probabilities λ_{ik} from condition (4).

In the following, we denote the position of vertex i by $\vec{i} \equiv \vec{r}_i$ and the vector from i to j by $\vec{ij} \equiv \vec{j} - \vec{i}$. Each triangle spanned by vertices j, k, l has the area A_{jkl} and an unnormalized normal $\vec{n}_{jkl} \equiv \vec{jk} \times \vec{jl}$. The set of points which lie within the plane spanned by the triangle's vertices j, k, l is consequently given by $\{\vec{r} \in \mathbb{R}^3 | \vec{n}_{jkl} \cdot \vec{r} = c_{jkl}\}$, with the constant $c_{jkl} \equiv \vec{n}_{jkl} \cdot \vec{j}$.

Lifting probabilities for case 2 (vertex hits surface). In case 2, the displacement $\vec{i} \to \vec{i} + d\vec{w}$ leads to a rejection because the triangle plane jkl is hit. Using the fact that $dE_{i,jkl} > 0$ (moving forward leads to a collision) and $dE_{j,ikl} < 0$, $dE_{k,ijl} < 0$, $dE_{l,ijk} < 0$ (if j, k, l are displaced by the same $d\vec{w}$, the collision will be avoided), simplifies eq. (3) and leads to

$$\lambda_{ij} = \frac{[-dE_{j,ikl}]^+}{[+dE_{i,jkl}]^+} = \frac{[+d\pi_{j,ikl}]^+}{[-d\pi_{i,jkl}]^+} . \qquad (5)$$

In order to obtain the differential changes of a Boltzmann weight $d\pi_{i,jkl}$, we consider the quantity $d_{i,jkl} \equiv \vec{n}_{jkl} \cdot \vec{i} - c_{jkl} = \vec{n}_{jkl} \cdot (\vec{i} - \vec{j})$, which is the signed distance from the active particle i to the triangle plane jkl multiplied by $2A_{jkl}$ (because $\vec{n}_{jkl}$ is unnormalized). Without loss of generality, we assume that $\vec{i}$ is directly above and $\vec{i} + d\vec{w}$ is directly below the triangular plane spanned by jkl; then, we can write down the Boltzmann weight for this specific infinitesimal move as $\pi_{i,jkl} = \Theta(d_{i,jkl})$ with the help of the Heaviside function $\Theta(x)$. This allows us to calculate the differentials

$$d\pi_{i,jkl} = dw \left.\frac{d}{dw}\right|_{w=0} \Theta(\vec{n}_{jkl} \cdot (\vec{i} + w\vec{e}_w - \vec{j})) ,$$

$$d\pi_{j,ikl} = -dw \left.\frac{d}{dw}\right|_{w=0} \Theta(\vec{n}_{j-w,k,l} \cdot (\vec{i} - \vec{j} + w\vec{e}_w)) .$$

Using the relations $\left.\frac{d}{dw}\right|_{w=0} \vec{n}_{j-w,k,l} = \vec{e}_w \times \vec{lk}$ and (5) yields $\lambda_{ij} = (\vec{e}_w \cdot \vec{n}_{ikl})/(\vec{e}_w \cdot \vec{n}_{jkl})$. The derivation shows that,

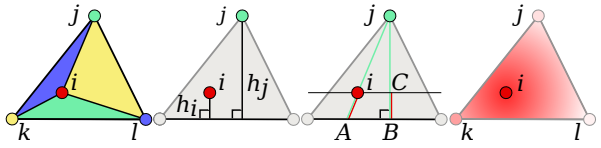

Fig. 2: As derived in (6), λ_{ij} is the ratio of the areas of the triangles shown. Both triangles share a base which is why λ_{ij} is also the ratio of the triangles' heights. Making use of the intersection theorem, λ_{ij} can be expressed as the ratio of $\overline{iA}$ to $\overline{jA}$ as well. λ_{ij} is moreover the same as the splitting probability of a particle that starts to diffuse from i (right).

exactly as for hard needles [11], the lifting probabilities are determined by the line derivatives of the distance $d_{i,jkl}$ from the active particle to the colliding hard object in the EC direction $\vec{e}_w$. As i, j, k, l lie all within a plane, $\vec{n}_{ikl}$ and $\vec{n}_{jkl}$ are parallel to each other, which is why

$$\lambda_{ij} = \frac{|\vec{n}_{ikl}|}{|\vec{n}_{jkl}|} = \frac{|\vec{ik} \times \vec{il}|}{|\vec{jk} \times \vec{jl}|} = \frac{A_{ikl}}{A_{jkl}} \,. \tag{6}$$

This means that the probability λ_{ij} to lift from i to one of the three vertices j is proportional to the area A_{ikl} formed with the two vertices k and l opposite to j, i.e., $\lambda_{ij} : \lambda_{ik} : \lambda_{il} = A_{ikl} : A_{ijl} : A_{ijk}$. Moreover, it implies that λ_{ij} is independent of the EC direction $\vec{e}_w$ (as for hard needles [11]). Fig. 2 illustrates two more different, but equivalent, geometric interpretations of this lifting probability:

$$\lambda_{ij} = \frac{A_{ikl}}{A_{jkl}} = \frac{h_i}{h_j} = \frac{\overline{iA}}{\overline{jA}} \left(= \frac{\overline{BC}}{\overline{jB}} \right) , \tag{7}$$

in which h_i and h_j are the heights to the opposite edge kl.

Lifting probabilities for case 3 (edge hits edge). It remains to discuss case 3, where a point on the edge im hits an edge jk of another triangle jkl, while vertex i is the active moving vertex. It leads to the same lifting rules as for case 2 with the vertex i hitting the surface exactly at the edge jk of the triangle jkl. The results (6) and (7) still apply, but lifting can only occur to vertices j or k ($A_{ijk} = 0$, $A_{ijl}, A_{ikl} > 0$). In this case, the lifting probabilities become proportional to the length ratios, $\lambda_{ij} = |\vec{ik}|/|\vec{jk}|$ and $\lambda_{ik} = |\vec{ij}|/|\vec{jk}|$ as for hard needles [11] (because triangles ijl and ikl have the same height from vertex l to edges ij or ik).

Lifting probabilities as splitting probabilities for diffusion on a hard object. – We are able to come up with an alternative derivation of the lifting probabilities, allowing us to attain a more intuitive understanding of the lifting process. As before, the first crucial step is to represent hard objects using a finite number of movable vertices (e.g., the three corner vertices for triangles). However, if two hard objects collide, the collision point will usually not coincide with a movable vertex, and we have to determine to which of the movable vertices to lift with which probability. If we subdivide the hard object into a mesh of auxiliary particles, which are immovable but can act as virtual or intermediate lifting partners from the neighboring positions, we find a peculiar analogy to diffusion: after contact, a virtual lifting process to the immediate neighbors of the contact site is started and continues to propagate through the mesh of immovable auxiliary particles like a random walk of the active particle. This random walk continues as long as no movable vertex, which is able to resolve the rejection by moving, is reached by the random walk. The lifting probability λ_{ij} to lift from the active colliding vertex i to the movable vertex j is thus exactly the *splitting probability* $P_j(\vec{i})$ of a random walk that starts at the collision site $\vec{i}$ and runs over the hard object, to reach the movable vertex j before reaching any other movable vertex [18], see fig. 2 (right).

This insight allows us to calculate the lifting probabilities for extended hard objects in a novel and straightforward manner. For hard needles, this approach is particularly easy because the lifting probability is simply the splitting probability of a 1D random walk with a specific starting position to reach a certain upper bound (the end of the needle) before a certain lower bound (the other end of the needle), also known in literature as the gambler's ruin problem [19]. This directly leads to the correct result $\lambda_{ij} = q = |\vec{ik}|/|\vec{jk}|$ and $\lambda_{ik} = 1 - q = |\vec{ij}|/|\vec{jk}|$ for the lifting probabilities from the collision point $\vec{i}$ to the two end points j and k of the needle [11].

For triangles, we can find the lifting probability to lift from the collision point $\vec{i}$ to vertex j as the splitting probability $P_j(\vec{i})$ to reach this vertex before reaching the vertices k or l from the starting position $\vec{i}$ confined on a triangular domain. This probability function needs to respect the conditions at the boundary, where only two of the vertices are movable, such that the edges of the triangle should, again, behave like needles. Additionally, the probability function value $P_j(\vec{i})$ at a position $\vec{i}$ inside the domain is given as the average over a region around that point. The probability function $P_j(\vec{i})$, thus, needs to be a harmonic function satisfying $\Delta P_j(\vec{i}) = 0$ (in which Δ is the Laplacian with respect to position $\vec{i}$). Because of the boundary conditions, the solutions need to be linear. The barycentric coordinates of the triangle both satisfy the boundary conditions and are harmonic functions, such that $\lambda_{ij} = P_j(\vec{i}) = A_{ikl}/A_{jkl}$ gives the probability of reaching vertex j before k and l from position $\vec{i}$, in complete agreement with (6).

Simulation details and results. – In order to compare triangles to other hard infinitely thin shapes, we use the two-dimensional packing fraction $\eta = \langle A \rangle^{3/2} N/V$. Periodic boundaries are applied to a box of volume $V = L^3$ in which the number N of triangles is varied. All triangles are initially equilateral with $a \equiv 1$ (i.e., we measure all lengths in units of the initial a in the following) and are allowed to vary their edge lengths by ± 0.3, as found to be

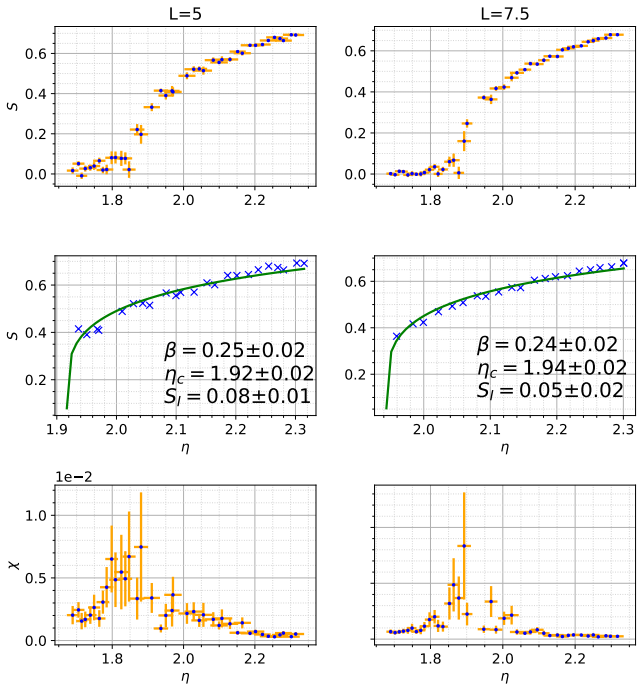

Fig. 3: Top: The nematic order parameter $\langle S\rangle$ as a function of the packing fraction η for different box sizes L. As η can vary during the simulation, the data points are not equidistant. Middle: The order parameter is fitted by a power law $S_I+(1-S_I)(1-\eta_c/\eta)^\beta$. Bottom: The susceptibility χ (variance of the order parameter) exhibits a maximum at the critical density.

quite effective for two-dimensional needles [11]. We simulate up to 1336 triangles for $L = 5$, and 4509 triangles for $L = 7.5$. During the simulation, the triangle ensemble deforms from equilaterality and exhibits mean values $(a_{\max} - a_{\min})/a_{\max} \approx 0.27$ corresponding to a mean minimum angle around 45°. The actual distribution of acute angles is peaked around a larger value of around 55°.

Nematic order parameter. A key quantity for liquid crystal ordering is the nematic order parameter S. Assigning to each triangle α its unit normal vector $\vec{n}^\alpha$ as orientation lets us analyze the order similarly as for rod-like liquid crystals. The nematic phase is associated with all triangle faces being parallel to each other. Therefore, the largest eigenvalue $\frac{2}{3}S$ of the tensor order parameter $Q_{ij} = N^{-1}\sum_\alpha n_i^\alpha n_j^\alpha - \frac{1}{3}\delta_{ij}$ is used to detect nematic order. The scalar order parameter S is determined by calculating all three eigenvalues $\lambda_+ \geq \lambda_0 \geq \lambda_-$ of Q. For systems that are axially symmetric around the director axis (the eigenvector of the largest eigenvalue λ_+), we have $\lambda_+ = \frac{2}{3}S$ and $\lambda_0 = \lambda_- = -\frac{1}{3}S$. As discussed in [14], the statistical error of S can be minimized if λ_0 is used for isotropic systems and λ_+ for nematic systems to measure $\langle S\rangle$, respectively (leading to $S \propto 1/N$ in the isotropic phase). We investigated order parameter distributions deep in the isotropic phase and find Gaussian distributions with $S < 0.1$ with $> 99\%$ confidence. We conclude that it is safe to use the eigenvalue $\lambda_0 = -S/3$ to determine S if $S < 0.1$ and to use $\lambda_+ = 2S/3$ otherwise. The scalar order parameter can also be written as $S = \frac{1}{2N}\sum_\alpha 3\cos^2\theta^\alpha - 1$ and the angle θ^α between $\vec{n}^\alpha$ and the director $\vec{d}$. We have $S = 0$ for an ideally isotropic system and $S = 1$ for perfectly nematic order.

The top of fig. 3 shows the mean order parameter $\langle S\rangle$ as a function of the packing fraction for two different system sizes L. Clearly, the triangle system exhibits an isotropic-nematic phase transition, which is smeared out by finite-size effects. Therefore, it is difficult to identify whether the transition is first or second order. In three dimensions however, we expect a discontinuous transition. The data in the nematic phase can be fitted by $S_I + (1 - S_I)(1 - \eta_c/\eta)^\beta$, where S_I is the order parameter value in the isotropic phase, and where we introduced a pseudo-critical exponent β, see fig. 3. We find pseudo-critical exponents $\beta \approx 0.24 - 0.25$ (in agreement with $\beta \approx 0.23$ in ref. [14]) and critical packing fractions $\eta_c \approx 1.91 - 1.96$.

Susceptibility. The ordering transition can be further characterized by studying the susceptibility $\chi = \langle S^2\rangle - \langle S\rangle^2$, which quantifies fluctuations of the nematic order parameter S. For n_{eff} effectively uncorrelated measurements, its uncertainty is $\sigma_\chi = \sqrt{2/(n_{\text{eff}} - 1)}\chi$ [20]. The susceptibility is shown at the bottom of fig. 3. The data exhibits a maximum of the susceptibility indicating a phase transition. The maximum is located close, but slightly below the values for the critical density $\eta_c \approx 1.91 - 1.96$ of the nematic phase transition as determined from order parameter fits.

Autocorrelation time and performance. Autocorrelation times of ECMC and local MC simulations give insights into the equilibration time and, thus, the performance of these algorithms. They also allow us to specify the number n_{eff} of effectively uncorrelated measurements correctly.

In order to compare the ECMC algorithm and a local MC algorithm regarding their performance, we use an elegant alternative to implementing a local MC algorithm for hard triangles from scratch: the EC displacement length w in the ECMC algorithm can be chosen so small that half of the ECs contain no lifting moves. This half of moves are, thus, seen as classical local MC moves that are accepted. Rejected local MC moves are certainly less effective than the other half of the moves that contain at least one lifting move. Therefore, it can be argued that a classical local MC simulation is at least as ineffective as our pseudo-local MC implementation.

We calculate the autocorrelation time from the autocorrelation function

$$C_S(\Delta t) = \sum_{t=0}^{n-\Delta t} \frac{(S_t - \langle S\rangle)\,(S_{t+\Delta t} - \langle S\rangle)}{(n - \Delta t)\sigma_S^2} \qquad (8)$$

of the order parameter S_t at simulation steps $t = 0, 1, 2, ..., n$. The integrated autocorrelation time is de-

Table 1: Comparison of autocorrelation times τ of the nematic order parameter S for different packing fractions between pseudo-local MC and ECMC algorithms (times measured in CPU time on identical hardware).

η	τ_{MC} / 10^3 s	τ_{EC} / 10^3 s	$\tau_{\mathrm{MC}}/\tau_{\mathrm{EC}}$
1.17 ± 0.02	0.314 ± 0.036	0.099 ± 0.007	3.2 ± 0.4
1.52 ± 0.02	2.00 ± 0.41	0.345 ± 0.031	5.8 ± 1.3
2.72 ± 0.03	3.87 ± 0.66	2.58 ± 0.32	1.5 ± 0.3
2.84 ± 0.03	8.27 ± 2.06	2.68 ± 0.32	3.1 ± 0.9

fined as $\tau = 1 + 2\sum_{\Delta t=1}^{M} C_S(\Delta t)$. The length M of the measurement window is determined by the phenomenological criterion $M = 5\tau$, which results in M-values that are sufficiently small to reduce errors but also large enough to remove biases in τ [21]. If the autocorrelation function exhibits a single exponential decay, the decay time is half the integrated autocorrelation time, $C_S(\Delta t) \sim e^{-2\Delta t/\tau}$. The integrated autocorrelation time directly determines the number $n_{\mathrm{eff}} = 1/\tau$ of effectively independent measurements [21], which enters our error analysis of simulation data.

We can measure the autocorrelation time also in CPU time (instead of simulation steps). Using identical hardware, this allows us to compare the performance of ECMC and local MC algorithms via their CPU time integrated autocorrelation times measuring the time they need to generate new decorrelated states. For $L = 5$, we find that ECMC autocorrelation times are smaller by factors $\sim 2-6$ compared to pseudo-local MC, see data in table 1.

Pressure. ECMC simulations also allow for an efficient determination of the pressure via [10]

$$\beta p a^3 = \rho a^3 + \left\langle \frac{\rho}{3w} \sum_{\text{lifts}} \frac{(\vec{r}_j - \vec{r}_i)^2}{(\vec{r}_j - \vec{r}_i)\cdot \vec{e}_w} \right\rangle, \qquad (9)$$

where $\vec{r}_j - \vec{r}_i$ is the particle distance at the collision triggering a lifting from i to j and where we have to sum over all lifting events along an EC. Equation (9) also takes into account a possible anisotropy of the system, which is obviously possible in the nematic phase. The resulting equation of state, i.e., pressure as a function of packing fraction, is shown in fig. 4 and exhibits a plateau around $\eta_c \sim 1.9$; this hints to the coexistence of two phases and, thus, a discontinuous transition. The location of the plateau is compatible with our previous result for η_c from the order parameter fits.

Comparison to discotic liquid crystals formed by hard platelets. Results of hard triangles are still lacking in the literature. There are, however, some publications of local MC simulations of infinitely thin circular platelets [14,17]. We find that the data yields similar results for the order parameter as a function of packing fraction if we assume that the diameter σ of the platelets is the counterpart of the average triangle height $\langle h \rangle$ in the definition of a packing fraction $\langle h \rangle^3 N/V$, see fig. 5.

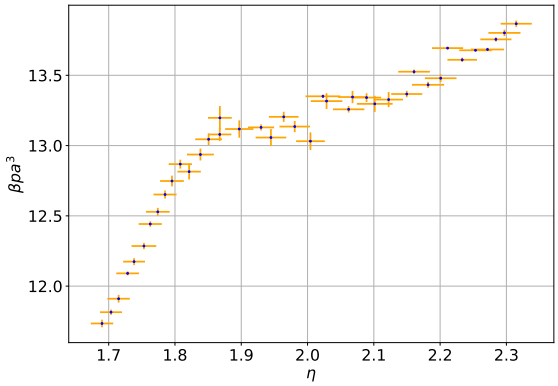

Fig. 4: Dimensionless pressure $\beta p a^3$ as a function of packing fraction η for $L = 5$. The plateau around $\eta_c \sim 1.9$ hints to a discontinuous isotropic-nematic transition.

From the theoretical point of view, it would be desirable to support this finding by comparing the excluded volume in the Onsager approach. The excluded volume of two platelets with a respective orientation of Ω is given by $|\sin\Omega|\sigma^3\pi/2$. The excluded volume of two triangles, however, depends on three angles defining their orientation (and not a single one), and for full generality, we had to provide a result taking into account different shapes and sizes of the triangles. For the special case of equilateral triangles having a height of $h = \sqrt{3}a/2$, we can quantify the average excluded volume for two triangles whose normals are tilted by an angle Ω with respect to each other, $V_{\mathrm{ex}} = (\frac{3\sqrt{3}}{4\pi} + \frac{3}{8})a^3|\sin\Omega| = (\frac{2}{\pi} + \frac{\sqrt{3}}{3})h^3|\sin\Omega|$. The excluded volume scales with h^3 rather than σ^3 as compared to platelets, thus, supporting the correspondence between h and σ.

Discussion. – We developed a rejection-free ECMC simulation of a liquid crystal system of infinitely thin triangles. In order to generalize existing ECMC algorithms from hard spheres and hard needles to planar triangles, we represent triangles by their three vertices resulting in effective 4-particle interactions. We derive the appropriate lifting probabilities that apply if a triangle vertex collides with the surface of a second triangle and prove maximal global balance for the ECMC algorithm. Our ECMC algorithm moves triangles by subsequent moves of the three vertices giving rise mainly to translation and facilitating rotation by a flexible tethered edge length. We do not include global rotations of triangles, which might be possible along the lines suggested for dimers [22] in future work. We showed that our novel ECMC algorithm is computationally more efficient than standard local MC simulations by comparing autocorrelation times in CPU time and find efficiency gains by factors of 2 to 6. In future research, there remains to be explored whether the ECMC speedup increases with system size as it has been found for hard-sphere [23] and for spin models [24].

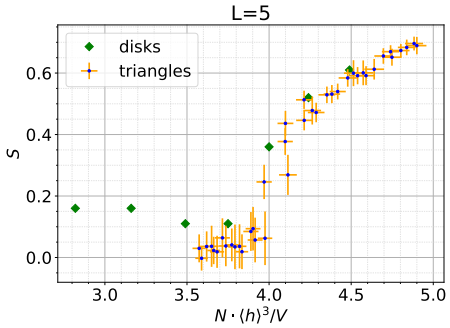

Fig. 5: The order parameter S from simulations of hard platelets (green diamonds, from ref. [14]) agrees with our simulation data for hard triangles if we identify the triangles' height h with the platelet's diameter σ.

The ECMC algorithm allows the simulation of triangle liquid crystal systems in the dense limit and explore the physics of liquid crystal ordering of these flat plate-like objects more efficiently than with local MC algorithms. Our triangle liquid crystal behaves very much like circular platelets, which are an important model system for discotic liquid crystals. In particular, we can compare to local MC simulations of circular infinitely thin platelets from refs. [14, 17]. The triangle liquid crystal exhibits an isotropic to nematic ordering transition above a critical packing fraction of $\eta_c \sim 1.9$, which we could successfully detect by the onset of nematic order parameter as quantified by the order parameter S (see fig. 3). The order parameter data (and susceptibility data) are inconclusive regarding the nature of the phase transition, while ECMC data for the pressure as a function of packing fraction exhibits a plateau that clearly hints at a discontinuous phase transition (see fig. 4).

We focused on the isotropic-nematic phase transition. Whether columnar phases can exist for systems of infinitely thin platelets such as the presented triangles remains an open question. The existence and structure of columnar phases have been a topic of much interest for platelets of finite (non-zero) thickness [25–29]. For infinitely thin platelets, the columnar phase is less stable as two parallel columns of infinitely thin platelets can slide into each other as in riffle shuffling, but columns of different orientation could still be stable at high packing fractions [30]. In order to answer this question, even higher packing fractions than those considered in this paper have to be explored.

Triangles are the simplest surface-like objects. Therefore, this work constitutes a first step in the development of ECMC algorithms for other flat particle shapes and for more complex extended triangulated surfaces. The ECMC lifting rules that we derived for single isolated triangles are applicable in the same form also for collisions with triangular surface elements of an extended surface consisting of many connected triangles. This paves the way to the use of the highly efficient ECMC technique to investigate the statistical physics of fluctuating surfaces and membranes.

REFERENCES

[1] Landau D. P. and Binder K., *A Guide to Monte Carlo Simulations in Statistical Physics* (Cambridge University Press, Cambridge) 2015
[2] Frenkel D. and Smit B., *Understanding Molecular Simulation: From Algorithms to Applications* (Academic Press, San Diego) 2002
[3] Metropolis N. *et al.*, *J. Chem. Phys.*, 1087-1092 **21** (1953)
[4] Hastings W. K., *Biometrika*, (1970) **57** 97-109
[5] Swendsen R. and Wang J., *Phys. Rev. Lett.*, **58** (1987) 86
[6] Wolff U., *Phys. Rev. Lett.*, **62** (1989) 361
[7] Bernard E. P. *et al.*, *Phys. Rev. E*, **80** (2009) 056704
[8] Krauth W., *Front. Phys.*, 663457 **9** (2021)
[9] Klement M. and Engel M., *J. Chem. Phys.*, 174108 **150** (2019)
[10] Michel M. *et al.*, *J. Chem. Phys.*, **140** (2014) 054116
[11] Harland J. *et al.*, *EPL (Europhysics Lett.)*, **117** (2017) 30001
[12] Kampmann T. A. *et al.*, *Front. Phys.*, 635886, **9** (2021)
[13] Höllmer P. *et al.*, *Comput. Phys. Commun.*, 107168 **253** (2020)
[14] Eppenga R. and Frenkel D., *Molecular Physics*, **52** (1984) 1303-1334
[15] Chandrasekhar S. and Ranganath G. S., *Reports Prog. Phys.*, **53** 57-84 (1990)
[16] Wöhrle T. *et al.*, *Chem. Rev.*, 1139-1241 **116** (2016)
[17] Bates M. A. and Frenkel D., *J. Chem. Phys.*, 6553-6559 **110** (1999)
[18] Redner S., *A Guide to First-Passage Processes* (Cambridge University Press) 2001
[19] Coolidge J. L., *Ann. Math.*, 181 **10** (1909)
[20] Rao C. R., *Linear Statistical Inference And Its Applications* 1973 (John Wiley & Sons, Inc., New York), p. 483
[21] Sokal A., *Functional Integration*, Vol. **361** 1997 (Springer, Boston), p. 131
[22] Guyon T. *et al.*, *J. Chem. Phys.*, **160** (2024) 024117
[23] Bernard E. P. *et al.*, *Phys. Rev. E*, 056704 **80** (2009)
[24] Michel M. *et al.*, *EPL (Europhysics Lett.)*, 20003 **112** (2015)
[25] Veerman J. A. C. and Frenkel D., (1992) *Phys. Rev. A*, **45** 5632-5648
[26] Chamoux A. and Perera A., *J. Chem. Phys.*, 8172-8181 **108** (1998)
[27] Duncan P. D. *et al.*,, *Phys. Rev. E*, 031702 **79** (2009)
[28] Wensink H. H. and Lekkerkerker H. N. W., *Mol. Phys.*, **20** 2111-2118 (2009)
[29] Wu L. *et al.*, *Mol. Phys.*, 1269-1288 **110** (2012)
[30] Marechal M. *et al.*, (2012) *Phys. Rev. Lett.*, **108** 206101